ISSN 0023-1584, Kinetics and Catalysis, 2007, Vol. 48, No. 4, pp. 521–534. © MAIK "Nauka/Interperiodica" (Russia), 2007.
Original Russian Text © A.G. Stepanov, V.N. Parmon, D. Freude, 2007, published in Kinetika i Kataliz, 2007, Vol. 48, No. 4, pp. 554–569.

MECHANISMS OF CATALYTIC REACTIONS

In Situ NMR Spectroscopy in Heterogeneous Catalysis: Kinetic Study of Hydrocarbon Conversion Mechanisms

A. G. Stepanov[a], V. N. Parmon[a], and D. Freude[b]

[a] *Boreskov Institute of Catalysis, Siberian Branch, Russian Academy of Sciences, Novosibirsk, 630090 Russia*
[b] *Department of Surface Physics, University of Leipzig, Leipzig, Germany*
e-mail: stepanov@catalysis.ru

Received March 23, 2006

Abstract—The potential of high-resolution solid-state NMR spectroscopy for kinetic and mechanistic studies of hydrocarbon conversion on solid acid catalysts between 20 and 300°C is considered. The use of this technique is illustrated by the elucidation of the mechanisms of hydrogen exchange and ^{13}C label transfer in alkanes and olefins, *n*-butane isomerization on sulfated zirconia, and ethane aromatization on zinc-containing zeolite beta. The kinetic parameters determined in these studies provide a basis for quantum chemical calculations of possible hydrocarbon activation and conversion pathways and for evaluating the reliability and accuracy of these theoretical calculations.

DOI: 10.1134/S0023158407040088

High-resolution solid-state NMR spectroscopy (MAS[1] NMR) has been used in the investigation of hydrocarbon conversion on the surface of heterogeneous catalysts for more than 20 years [1, 2]. The progress in the development and application of this experimental technique has greatly influenced the understanding of heterogeneous catalytic reactions. NMR has revealed many processes occurring on the surface of acid catalysts. Furthermore, NMR has identified a number of intermediates that play a significant role in hydrocarbon activation and conversion but are "invisible" to conventional ex situ methods. For example, in 1989, aromatic hydrocarbons of certain composition and structure were identified in methanol conversion into motor fuel on zeolite HZSM-5. These hydrocarbons result from the main reactions and reside in zeolite pores. Earlier, they were not identified among the main products leaving the reactor [3]. Thus, the in situ NMR identification of reaction products in the zeolite pores confirmed that the molecular sieve effect takes place in this process.

In situ NMR revealed the formation of a number of alkoxides that are now viewed as important intermediates in hydrocarbon conversion on acid catalysts. Isopropoxide was the first among the alkoxides identified and characterized in 1989 [4]. This was followed by the identification of methoxy [5, 6], ethoxy [6, 7], isobutoxy [8], and *tert*-butoxy [9] intermediates.

The same method revealed the formation of stable carbocationic intermediates, such as alkyl-substituted cyclopentenyl cations, in the conversion of olefins [4, 10], alcohols [11, 12], and alkanes [13]. Cyclic carbonium ions were identified in hydrocarbon conversion reactions in the presence of carbon monoxide [14]. *N*-alkylnitrilium cations were found to be intermediates in the reactions between an olefin or alcohol and a nitrile [15, 16].

In 1994, NMR spectroscopy made it possible to observe the activation of lower alkanes on a zeolite catalyst: carbon label transfer from a methyl group to the methylene group of propane was observed on zeolite HZSM-5 above 250°C [17].

The NMR studies of hydrocarbon isomerization and cracking over the last 15 years have demonstrated that these reactions on solid acid catalysts proceed via a conjugated polymerization mechanism (Scheme 1) [4, 12, 13, 18–21]. This mechanism is similar to the mechanism of the conjugated polymerization of olefins in concentrated sulfuric acid, a reaction discovered by Ipatieff as early as the 1930s [22]. In conjugated polymerization, the formation of main cracking and isomerization products is accompanied by a buildup of alkyl-substituted cyclopentenyl cations on the catalyst surface. These cations deactivate the catalyst. It is these cations that are the precursors of the fused arenes that form on the catalyst surface. Raising the reaction temperature can convert these arenes into simpler aromatic compounds, such as benzene, toluene, and xylenes [19].

In all of the above examples, the reaction mechanism or the nature of the intermediates was deduced from an in situ analysis of the reaction products on the catalyst surface. This approach has developed into kinetic studies by in situ MAS NMR spectroscopy, which can provide important information concerning the mechanisms of heterogeneous reactions involving hydrocarbons. In this method, reaction mechanisms are

[1] MAS = magic angle spinning.

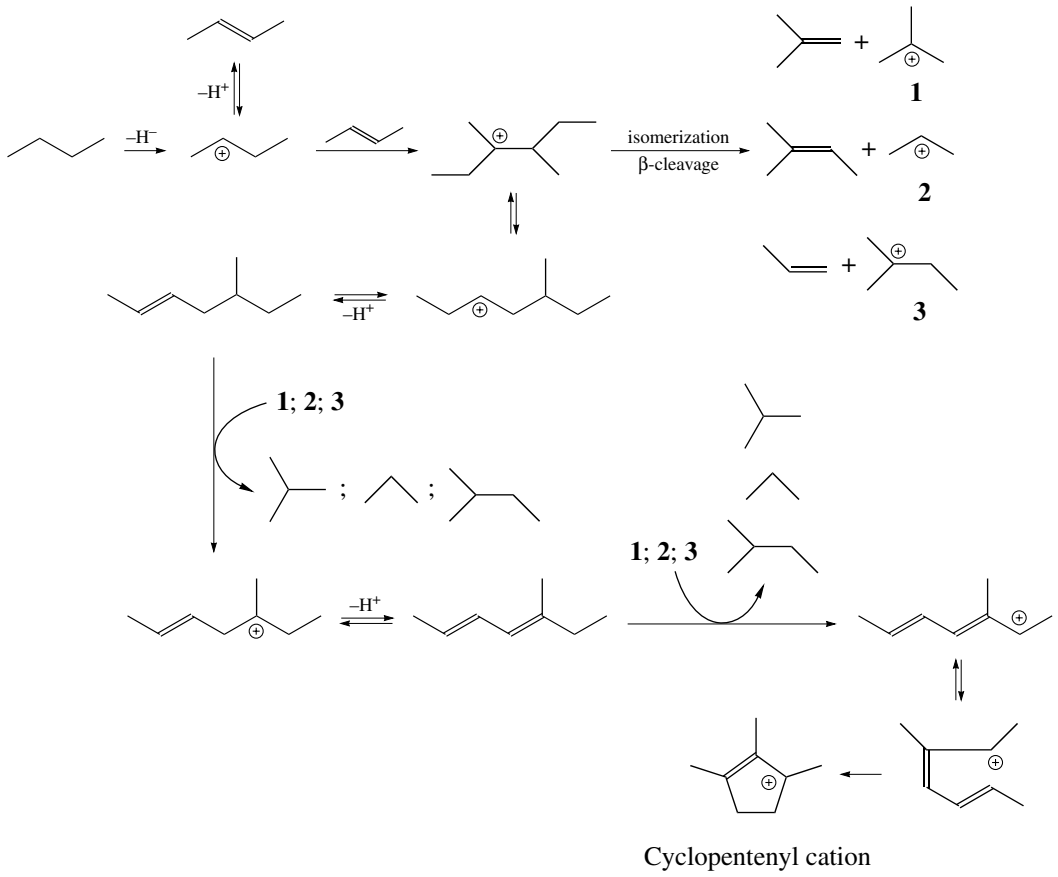

Scheme 1. Mechanism of the conjugated polymerization of *n*-butane on sulfated zirconia (according to ^{13}C MAS NMR data [20]).

elucidated not through spectroscopic identification of intermediates, but through kinetic investigation of the reaction examined and through determination of its kinetic parameters. It is significant that the parameters thus determined can serve as the basis for the verification of quantum chemical calculations for molecule activation and conversion pathways.

SPECIFIC FEATURES OF KINETIC MEASUREMENTS BY IN SITU MAS NMR

Kinetic measurements by in situ MAS NMR are rather laborious. As a rule, hydrocarbon conversions on a catalyst surface occur at rather high temperatures. For this reason, the NMR probe, which contains a rapidly spinning sample, must be maintained at a high temperature throughout the reaction time. Therefore, high-temperature NMR probes are required.

Figure 1 schematizes kinetic measurements by in situ solid-state MAS NMR. The reactor used in this technique is a highly axisymmetric glass tube with a volume of 0.05–0.1 ml. A catalyst sample is placed in this tube. After proper conditioning of the sample and reactant adsorption, the tube is sealed. The reaction takes place in a static microreactor inside a zirconia rotor. The rotor, with the sample, is placed into the probe of an NMR spectrometer. The reaction to be examined is initiated by raising the sample temperature. The spinning of the sample at a frequency of 2–10 kHz at the magic angle ($\theta = 54.7°$) to the direction of the external magnetic field B_0 at the preset reaction temperature narrows the signal from the adsorbed hydrocarbons to a sufficient extent. By monitoring the signals from individual fragments of the molecule during the reaction, it is possible to trace the kinetics of the conversion of the hydrocarbon molecule as a whole and of the individual fragments. Note that, at 300°C, the gas pressure in the sealed glass reactor can reach 20 bar.

MECHANISM OF HYDROGEN EXCHANGE BETWEEN PROPANE AND THE ACID ZEOLITE HZSM-5

In 1998, we established that hydrogen atom exchange between deuterated propane and the acid groups of the zeolite strengthens the signals from the methyl and methylene groups in the ^{1}H NMR spectrum of adsorbed propane [23]. An analysis demonstrated that the apparent rate constants and activation energies (E_a) of hydrogen exchange for the methyl and methyl-

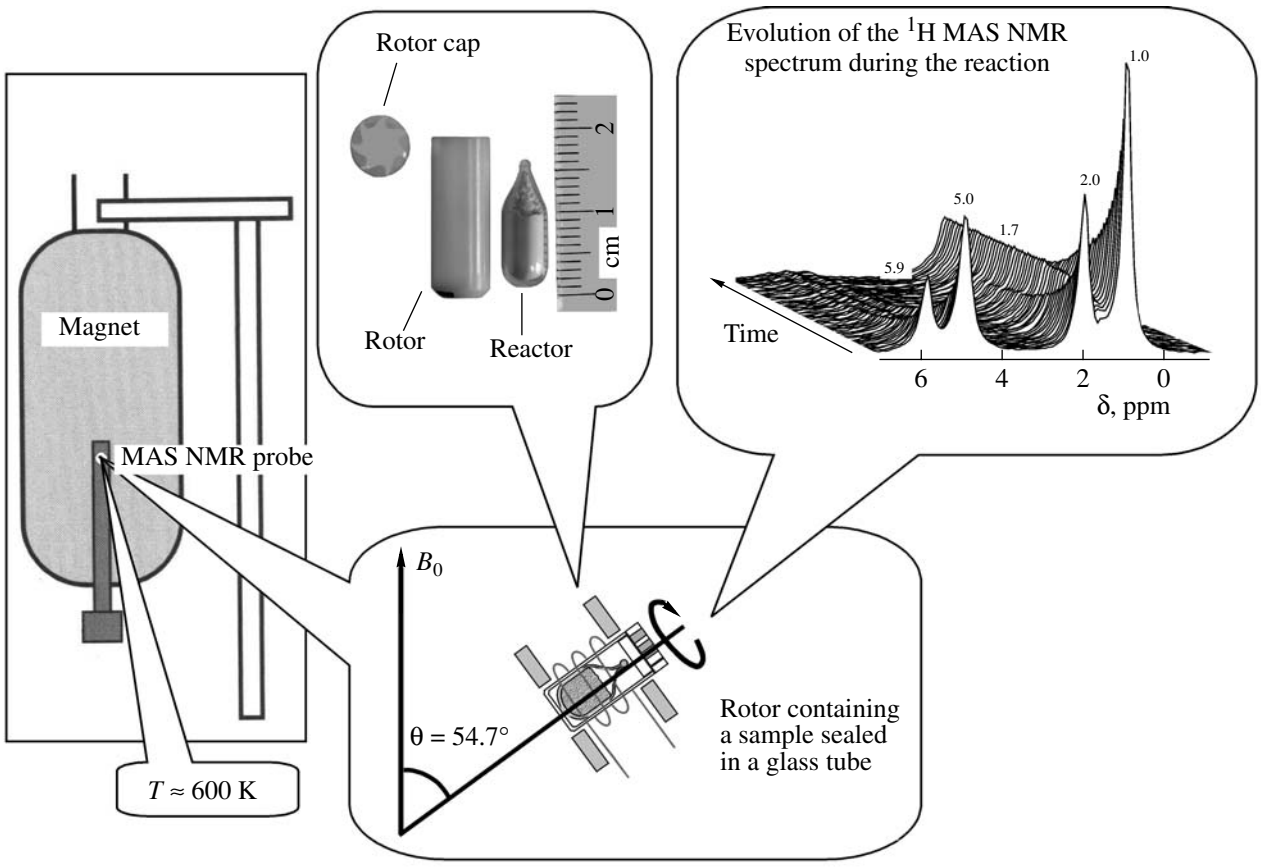

Fig. 1. Schematic of the MAS NMR technique for in situ kinetic studies of reactions on a solid catalyst surface.

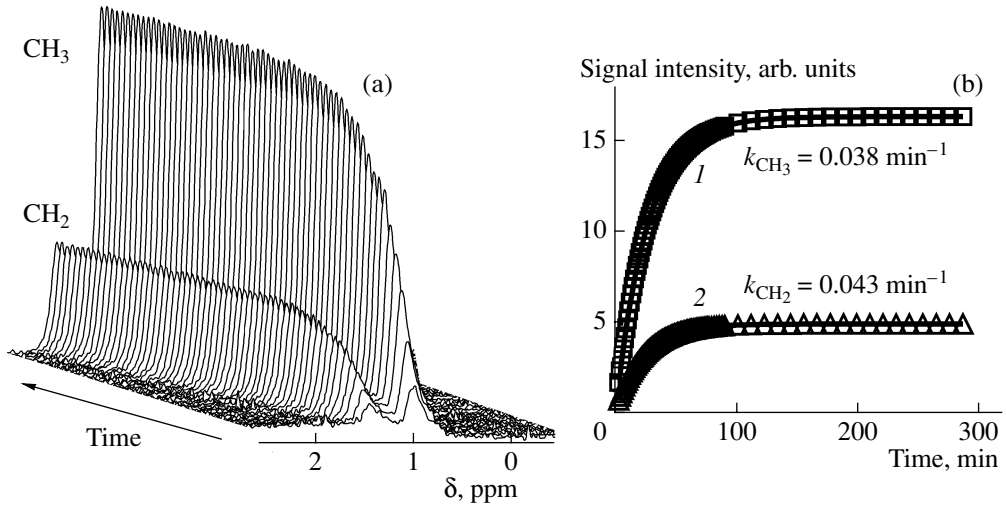

Fig. 2. (a) Time variation of the ^{1}H MAS NMR signals from the methyl and methylene groups of propane-d_8 adsorbed on zeolite HZSM-5. (b) Kinetics of protium transfer from the acid OH groups of the zeolite to (*1*) the methyl groups and (*2*) the methylene group of propane at 519 K. The solid lines correspond to the rate constants indicated at the curves.

ene groups are similar: E_a = 108 and 117 kJ/mol, respectively (Fig. 2). By that time, the activation energy of hydrogen exchange between ethane and the Brønsted acid sites of zeolites had already been estimated under the assumption that the reaction proceeds via a concerted mechanism to yield a pentacoordinated carbon atom as the transition state [24]. From our kinetic data and these estimates [24], we inferred that the methyl

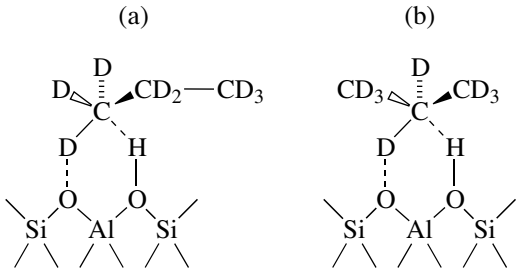

Scheme 2. Transition states in direct H–D exchange between the AlOHSi acid groups of zeolite HZSM-5 and the (a) CD_3 and (b) CD_2 groups pf propane-d_8.

and methylene hydrogen atoms are independently involved in the direct exchange with the Brønsted acid sites of the zeolite and this yields a pentaccordinated carbon atom as the transition state (Scheme 2).

The above studies were followed by investigation of hydrogen exchange between propane and sulfated zirconia promoted with aluminum oxide (Al_2O_3/SZr) [25]. A reaction involving propane with selectively deuterated methyl groups was studied, and the signals from the methyl groups in the ^1H NMR spectrum were observed to grow during the reaction, while the signal from the methylene group remained invariable. Therefore, the reaction in this system involves only the methyl hydrogen atoms of propane; that is, hydrogen exchange is regioselective. In the reaction involving completely deuterated propane, the exchange rate for the methyl groups at 355 K is approximately twice as high as the exchange rate for the methylene group (Fig. 3). The regioselectivity of isotope exchange in this system is illustrated by Scheme 3. The key intermediate in this reaction is the isopropyl cation, which is in equilibrium with propylene. Olefin protonation by the acid sites of the catalyst and cation deprotonation carry out hydrogen exchange only in the methyl groups (Scheme 3, process 1). The much smaller extent of H–D exchange in the methylene group is explained by intramolecular exchange in the adsorbed isopropyl cation (Scheme 3, process 2).

Based on the results obtained for H–D exchange in propane on Al_2O_3/SZr, we assumed that Scheme 3 is also applicable to the same reaction on the HZSM-5 catalyst, for which the exchange rates for the methyl and methylene groups are equal [23]. However, it is essential here that the rate of intramolecular exchange (process 2) should be much higher than the rate of the direct exchange of the acid hydroxyl protons of the catalyst for the methyl protons of adsorbed propane (process 1).

In order to refine the exchange mechanism and choose between Schemes 2 and 3, we carried out a

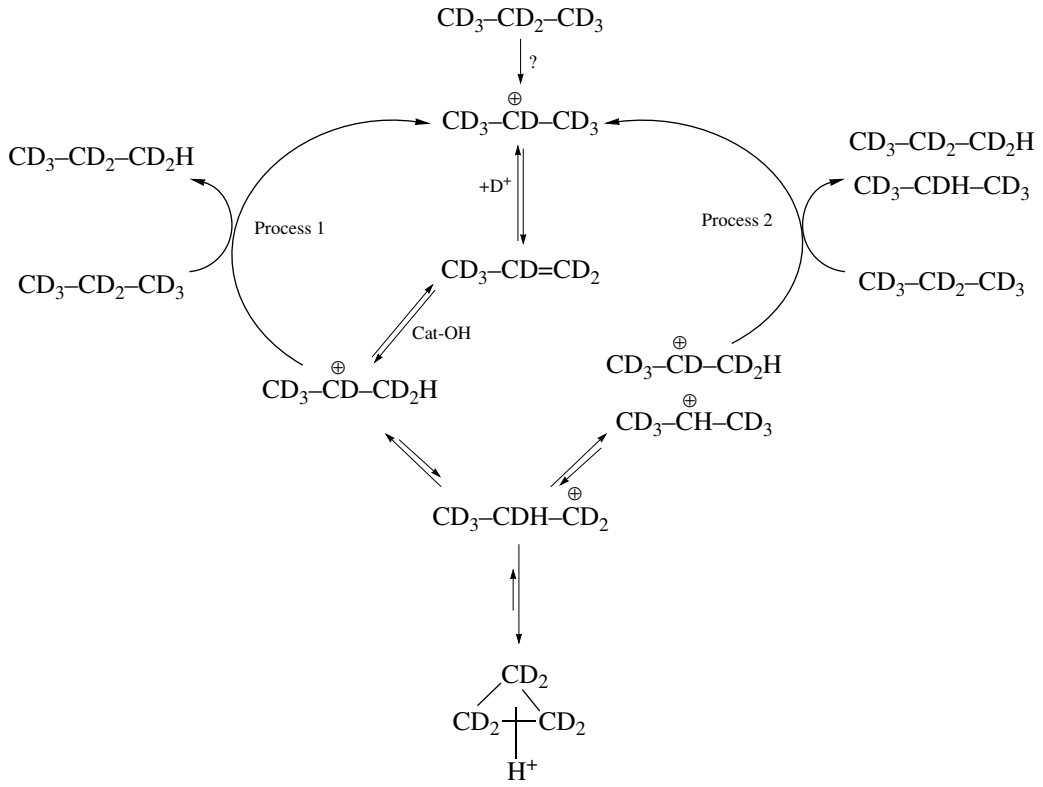

Scheme 3. Catalytic cycle responsible for the regioselectivity of H–D exchange (process 1) and for the loss of exchange regioselectivity through the skeletal isomerization of propane-d_8 (process 2) on solid acid catalysts (based on data reported in [23]).

kinetic study of this reaction using three different propanes, namely, propane in which both methyl groups are deuterated, propane in which the methylene group is deuterated, and completely deuterated propane. In this study, we checked the fit between the observed kinetics and possible hydrogen exchange kinetic schemes. We considered the consecutive, parallel, and cyclic exchange mechanisms (Scheme 4). Obviously, if the kinetic scheme is chosen correctly, the rate constant values fitted to the observed kinetic curves will be the same for all of the three differently deuterated propanes. A numerical analysis of the kinetic curves demonstrated that this criterion is satisfied only by the cyclic mechanism. Indeed, for the consecutive mechanism, the rate constants of exchange in the methyl group (k_1) and intramolecular exchange (k_3) vary widely from one deuterated propane to another (table). By contrast, for the cyclic mechanism, the rate constants k_1, k_2, and k_3 are approximately the same for all of the three propanes. Furthermore, for the cyclic mechanism and T = 553 K, the fitted rate constant of direct exchange between hydroxyl groups and the methyl groups (k_1) is ~1.5 times larger than the fitted rate constant of exchange between hydroxyl groups and the methylene group (k_2). At the same time, intramolecular hydrogen transfer (k_3) is ~5 times slower than the exchange between the OH groups of the catalyst and the methyl groups.

Thus, we can confirmed our earlier inference that H–D exchange in the methyl and methylene groups of propane is mainly due to direct proton transfer from the acid sites of the zeolite [23]. The small values of the intramolecular exchange rate constant are evidence that the consecutive mechanism of hydrogen exchange [25, 26] is not valid for propane on HZSM-5.

The kinetics of intramolecular ^{13}C label transfer from the methylene group of propane to its methyl groups was studied by ^1H NMR [27] and ^{13}C NMR [28, 29]. It was found that the rate of the intramolecular transfer (scrambling) of carbon atoms is two times lower than the intramolecular hydrogen transfer rate. However, the activation energies of these processes are approximately equal (Fig. 4). Similar intramolecular carbon scrambling and hydrogen transfer kinetics were observed for the isopropyl cation in a superacid solution [30]: the apparent activation energies of carbon scrambling and intramolecular hydrogen transfer were equal, and the hydrogen transfer rate was nearly thrice as high as the carbon scrambling rate. The similarity between the carbon and proton transfer kinetics in the superacid and those on the zeolite suggests that carbon and proton scramblings proceed via the formation of the same isopropyl cation. The kinetic parameters determined for the carbon and hydrogen scrambling elementary reactions can be used in the quantum chemical calculation of the propane activation and conversion pathways on acid zeolites.

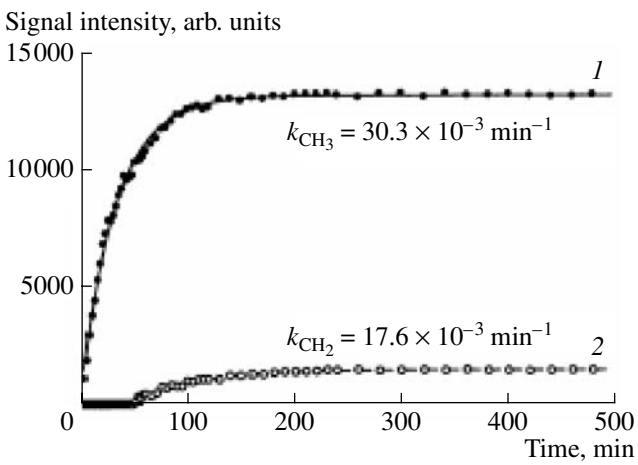

Fig. 3. Time variation of the ^1H MAS NMR signals from (*1*) the methyl groups and (*2*) the methylene group of propane-d_8 adsorbed on Al_2O_3/SZr. The observed exchange rate constant [25] is indicated at each curve. T = 355 K.

Consecutive mechanism

$$CD_3–CD_2–CD_3 + OH \underset{}{\overset{k_1}{\rightleftharpoons}} CD_2H–CD_2–CD_3 + OD \overset{k_3}{\rightleftharpoons} CD_3–CDH–CD_3 + OD$$

Parallel mechanism

$$CD_3–CD_2–CD_3 + OH \begin{array}{l} \overset{k_1}{\rightleftharpoons} CD_2H–CD_2–CD_3 + OD \\ \underset{k_2}{\rightleftharpoons} CD_3–CDH–CD_3 + OD \end{array}$$

Cyclic mechanism

$$CD_3–CD_2–CD_3 + OH \begin{array}{l} \overset{k_1}{\rightleftharpoons} CD_2H–CD_2–CD_3 + OD \\ \underset{k_2}{\rightleftharpoons} \quad\quad \updownarrow k_3 \\ \quad\quad CD_3–CDH–CD_3 + OD \end{array}$$

Scheme 4. Possible mechanisms of hydrogen exchange between deuterated propane and the undeuterated acid groups of zeolite HZSM-5.

Hydrogen exchange rate constants for deuterated propanes on zeolite HZSM-5 determined by fitting experimental data to the kinetic schemes presented in Scheme 4

Deuterated propane	T, K	Reaction scheme*						
		consecutive		parallel		cyclic		
		k_1	k_3	k_1	k_2	k_1	k_2	k_3
Propane-d_8	553	4	>18	3.6	2.4	3.4	2.3	0.6
Propane-1,1,1,3,3,3-d_6	556	8	0.55	11.9	5.8	4.5	2.4	0.6
Propane-2,2-d_2	552	0–100	2.0	3.6	4.0	3.4	2.7	0.6

* The dimension of a rate constant is 10^{-5} g μmol^{-1} min^{-1}.

TRANSFER OF A SELECTIVE ^{13}C LABEL IN AN OLEFIN ADSORBED ON FERRIERITE

Ferrierite (HFER) is known to be an efficient zeolite catalyst for *n*-butene isomerization into isobutene. In situ NMR studies of this reaction revealed the transfer of the ^{13}C label from a CH group of butene to its methyl group at ~323 K. Note that no other butene conversions take place at this temperature [31]. In the ^{13}C NMR spectrum of adsorbed *n*-butene-2 labeled in the 2-position, the signal from the CH group at 126 ppm decreases with time and the signals from the methyl groups of the *cis* and *trans* isomers of *n*-butene-2 at 13 and 17 ppm increase with time (Fig. 5) because of the transfer of the ^{13}C label.

The mechanism of the intramolecular transfer of a ^{13}C label in olefins has not been reliably elucidated as yet. What is known for certain is that this transfer takes place in intermediate carbenium ions. Hence, we infer that ^{13}C transfer in *n*-butene-2 adsorbed on ferrierite is also a consequence of the formation of the *sec*-butyl cation from *n*-butene [31]. The formation of protonated cyclopropane from this cation can result in carbon transfer. An analysis of the kinetics of ^{13}C transfer (scrambling) in *n*-butene on ferrierite at various temperatures (Fig. 6) enabled us to estimate the activation energy of this process.

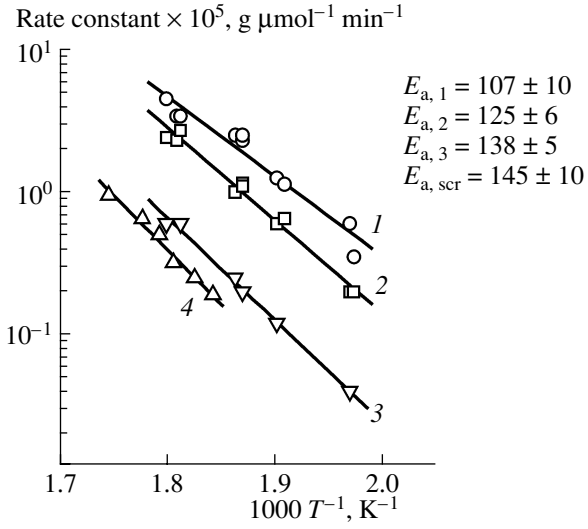

Fig. 4. Arrhenius plots of the rate constants (*1*) k_1, (*2*) k_2, and (*3*) k_3 for the cyclic mechanism of H–D exchange in deuterated propane and (*4*) the rate constant of ^{13}C label transfer in CH_3–$^{13}CH_2$–CH_3 (k_{scr}) on zeolite HZSM-5. $E_{a,1}$, $E_{a,2}$, $E_{a,3}$, and $E_{a,scr}$ are the apparent activation energies (kJ/mol) [29].

From the potential energy profile for the carbon label transfer reaction, the apparent activation energy of this reaction, and earlier data indicating that carbonium ions can be stable in zeolites [32, 33], we deduce that the true activation energy of carbon scrambling ($E_{a,scr}$) in *n*-butene can exceed 100 kJ/mol (Fig. 7). This value is larger than the activation energy of the same process in a liquid superacid [34] by a factor greater than 3. In view of this, it would be very pertinent to carry out a theoretical analysis of the possible pathways of ^{13}C transfer in olefins adsorbed on zeolites. The kinetic parameters that we determined can serve as the basis for quantum chemical calculation of the possible pathways of ^{13}C transfer in olefins on acid sites of zeolites and can be used as a kind of reference in estimating the accuracy of computational methods.

n-BUTENE ISOMERIZATION ON SULFATED ZIRCONIA

Sulfated zirconia is known to be an efficient catalyst for low-temperature isomerization of *n*-butane into isobutane. It was demonstrated by conventional ex situ methods that, at the early stages of this reaction, when the only observable product is isobutane, isomerization proceeds via a monomolecular mechanism. The appearance of butane disproportionation products, namely, propane and pentanes, during the reaction indicates a crossover from the monomolecular mechanism to a bimolecular mechanism [35].

In situ NMR monitoring of the isomerization product concentrations has provided a much deeper insight into the mechanism of the isomerization reaction. The in situ monitoring of the isomerization kinetics of *n*-butane with a selectively ^{13}C-labeled methyl group

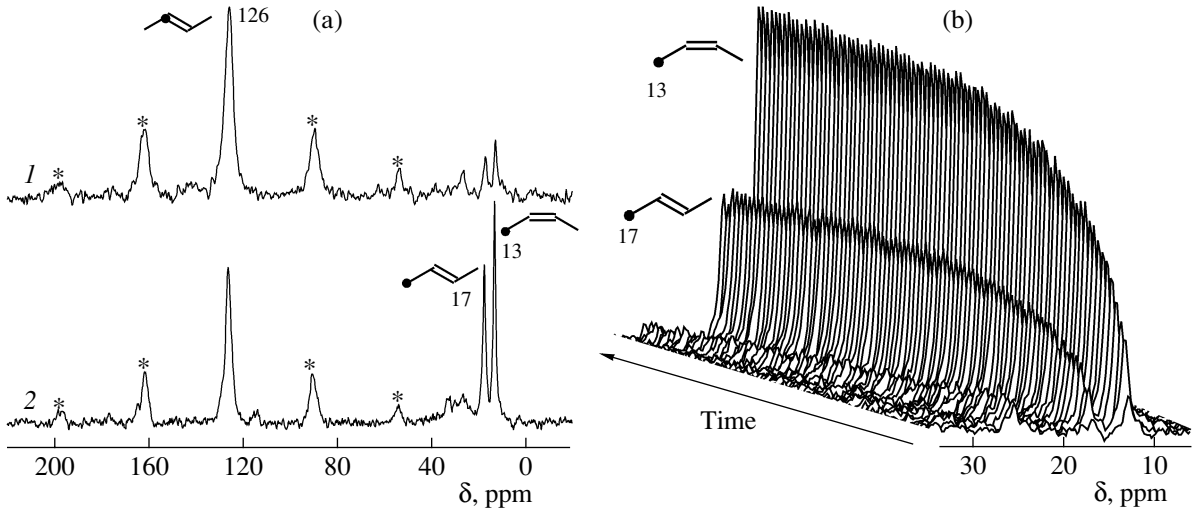

Fig. 5. (a) ^{13}C MAS NMR spectra of *n*-butene-2 labeled in the 2-position on ferrierite. The spectra are recorded after the sample is held at 323 K for (*1*) 17 min and (*2*) 20 h. (b) Evolution of the ^{13}C MAS NMR spectrum in the region of methyl groups during the reaction at 323 K. Here and in the figures presented below, the stars label the lines that result from sample spinning with a speed insufficient to average out the chemical shift anisotropy of the observed signals.

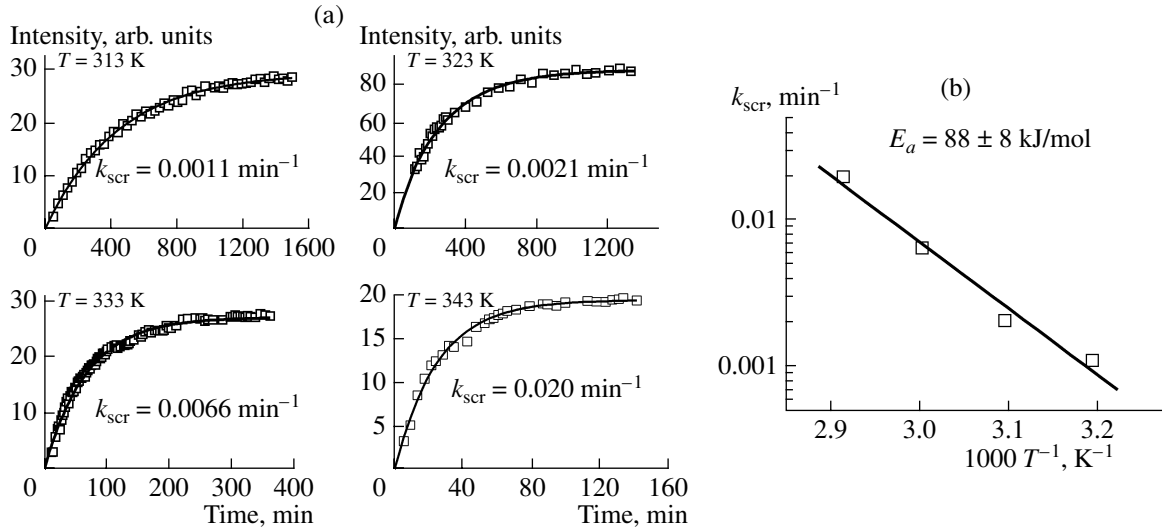

Fig. 6. (a) Kinetics of the scrambling of the ^{13}C atoms from the –CH= groups to methyl groups in *n*-butene-2 labeled in the 2-position on ferrierite. (b) Arrhenius plot of the apparent scrambling rate constant k_{scr}.

indicates a progressive weakening of the signal from this group (14.7 ppm) and a progressive strengthening of the signal from isobutane (26.0 ppm) during the reaction (Fig. 8). This is accompanied by a strengthening of the signal from the methylene group of *n*-butane (27.1 ppm) [36]. This signal reaches its maximum 100 min after the beginning of the reaction and then weakens. The growth and decline of the signal at 27.1 ppm indicates the transfer of the ^{13}C label (carbon scrambling) from the methyl group to a methylene group of butane. This carbon scrambling in butane accompanies isomerization. Thus, in situ NMR enables the researcher to monitor the kinetics of both isomerization and carbon scrambling.

An analysis of the mass spectra of the starting hydrocarbon and the hydrocarbons desorbed from the catalyst surface 3 h after the beginning of the reaction demonstrated that both initial *n*-butane and *n*-butane resulting from the reaction have a single ^{13}C label. At the same time, isobutane, the isomerization product, contains two carbon labels (Fig. 9). Note that the two labels in isobutane are detected at the reaction stage at which this hydrocarbon is the only observable product and butane disproportionation has not set in [20].

The presence of two labels in isobutane and a single label in *n*-butane suggests that scrambling in *n*-butane is certainly a monomolecular process (Scheme 5, pathway 1), while isomerization itself is a purely bimolecu-

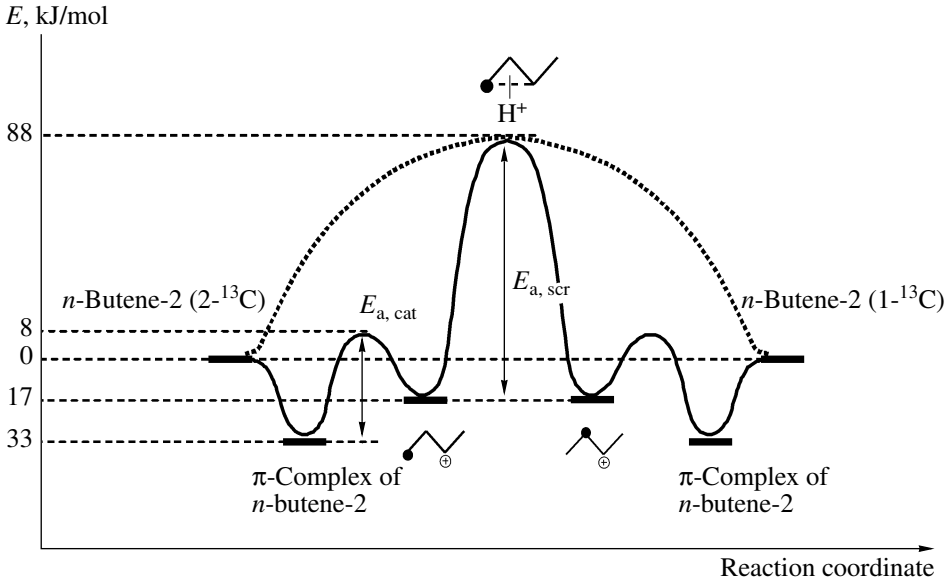

Fig. 7. Potential energy profile for ^{13}C label transfer in *n*-butene-2 on an acid zeolite (ferrierite).

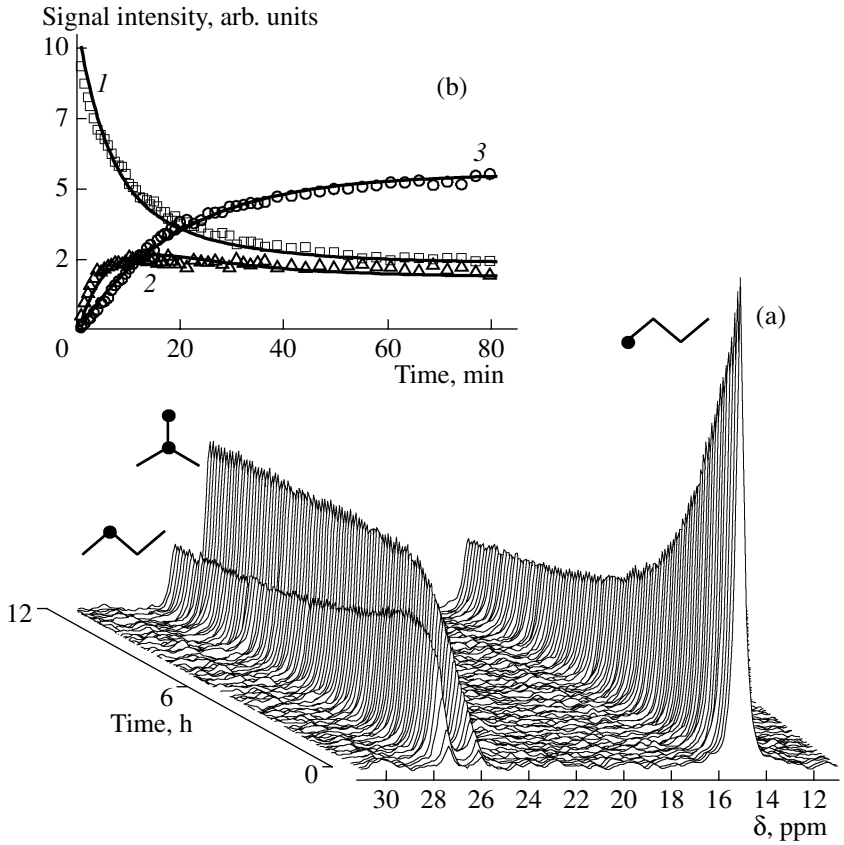

Fig. 8. (a) Time evolution of the ^{13}C MAS NMR spectrum of *n*-butane labeled in the 1-position on sulfated zirconia. (b) Kinetic curves for (*1*) *n*-butane labeled in the 1-position, (*2*) *n*-butane labeled in the 2-position, and (*3*) isobutane labeled in the 1- and 2-positions. The reaction temperature is 313 K.

lar process (Scheme 6). The monomolecular isomerization mechanism (Scheme 5, pathway 2) does not take place on sulfated zirconia. Our bimolecular *n*-butane isomerization mechanism (Scheme 6) explains why *n*-butane initially containing one ^{13}C label yields isobutane with two ^{13}C labels.

An analysis of *n*-butane isomerization kinetics at 291–323 K demonstrated that the observed rate con-

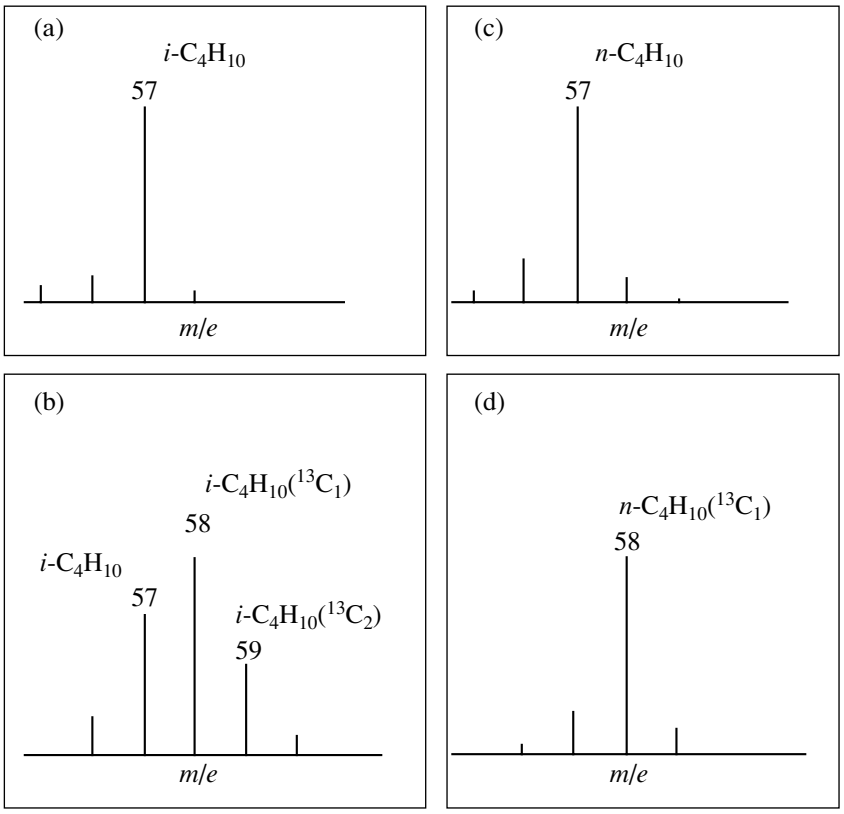

Fig. 9. Mass spectra: (a) unlabeled isobutane; (b) isobutane that has resulted from the isomerization of *n*-butane labeled in the 1-position, recorded 3 h after the beginning of the reaction; (c) unlabeled *n*-butane; (d) *n*-butane that has formed from *n*-butane labeled in the 1-position, recorded 3 h after the beginning of the reaction.

stants of monomolecular carbon scrambling are twice as large as the rate constants of bimolecular isomerization and that the apparent activation energies of these reactions are similar (71 and 63 kJ/mol, respectively) [36].

Thus, these NMR studies led us to conclude that *n*-butane isomerization is a bimolecular process probably including the formation of a sec-butyl cation, the dimerization of this cation, the isomerization of the resulting dimer, and the cracking of the latter. This is the route leading from *n*-butane with a single ^{13}C label to isobutane with two ^{13}C labels.

HYDROGEN EXCHANGE OF METHANE AND ETHANE WITH THE ZINC-CONTAINING ZEOLITE ZnHBEA

Zinc-containing high-silica zeolites are efficient catalysts for aromatization of lower alkanes [37–40]. There have been many studies dealing with the activation and conversion mechanisms of lower alkanes and with the state of zinc in these catalysts. V.B. Kazanskii and his colleagues have recently discovered strong adsorption complexes between lower alkanes (methane and ethane) and zinc cations [41–43]. Zinc–alkyl frag-

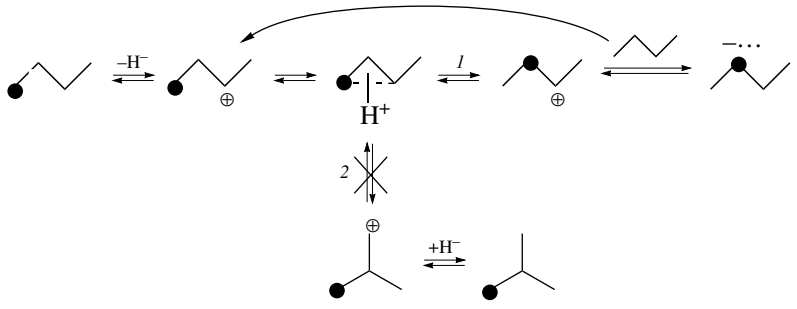

Scheme 5. Monomolecular mechanism of the transfer of the ^{13}C label in *n*-butane on SZr (pathway 1). The black points are ^{13}C atoms. The monomolecular isomerization mechanism (pathway 2) does not take place.

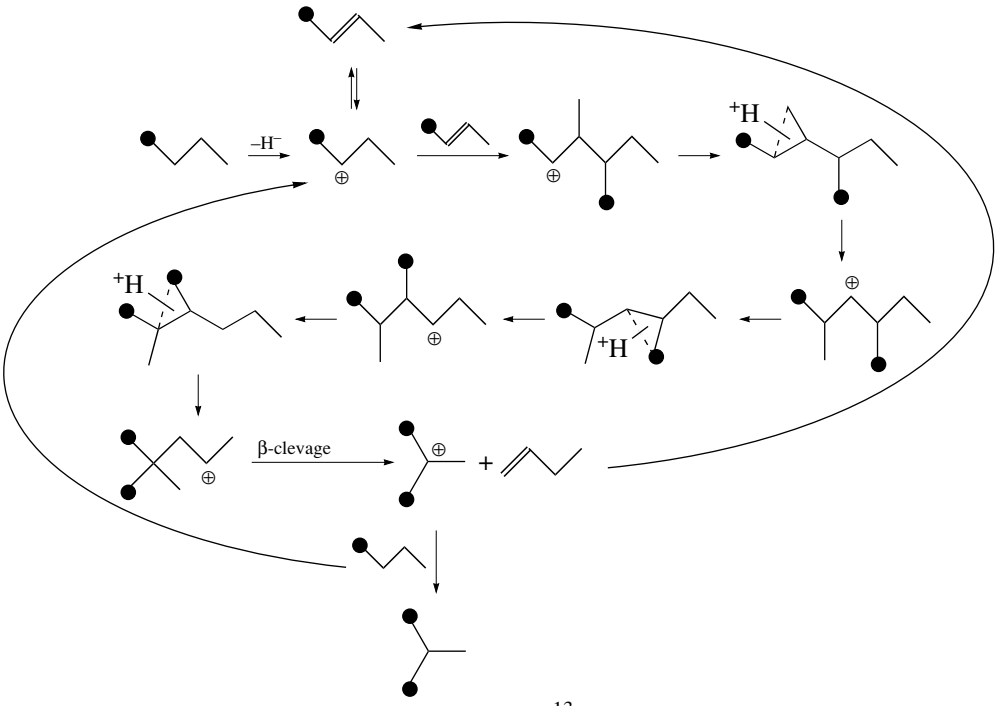

The black points are ^{13}C atoms.

Scheme 6. Bimolecular mechanism of the skeletal isomerization of *n*-butane on SZr.

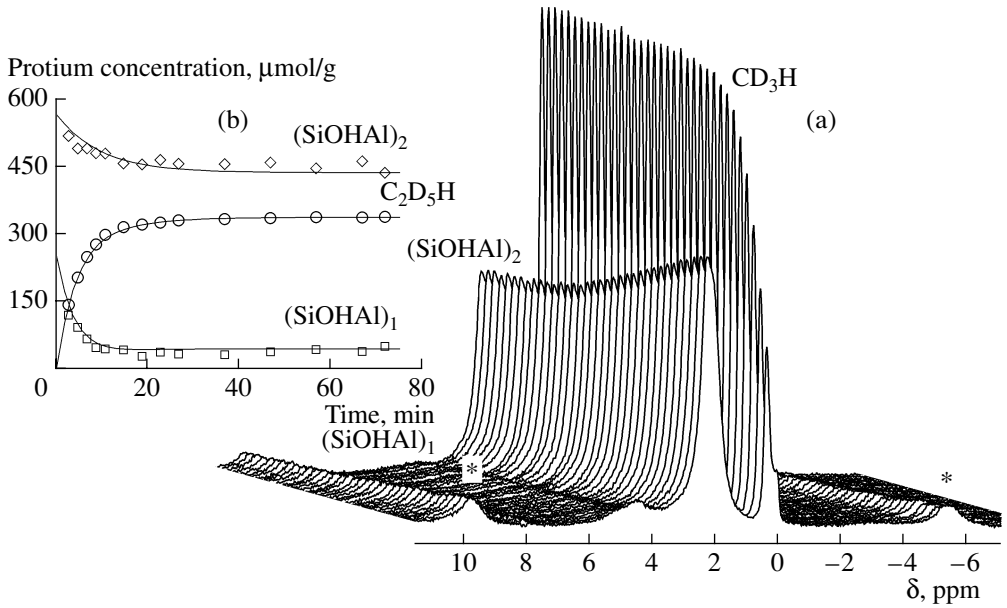

Fig. 10. (a) Time evolution of the signals from methane and the acid OH groups of the zeolite at 508 K in the ^1H MAS NMR spectrum of methane-d_4 adsorbed on zeolite ZnHBEA. (b) Kinetics of protium transfer from the OH groups of the zeolite to the ethane-d_6 molecule at 538 K.

ments form from these complexes on the catalyst surface at an elevated temperature.

Kinetic NMR studies of the activation of lower alkanes have demonstrated that the hydrogen exchange temperature for methane and ethane on the zinc-containing zeolite ZnHBEA is 200–250 K below the hydrogen exchange temperature for the pure acid forms of high-silica zeolites [44–46]. During methane-d_4 (ethane) adsorption between 420–520 K, the signal from the methane (ethane) protons grows owing to protium transfer from acid groups of the zeolite to molecules of the deuterated alkane (Fig. 10). This is accom-

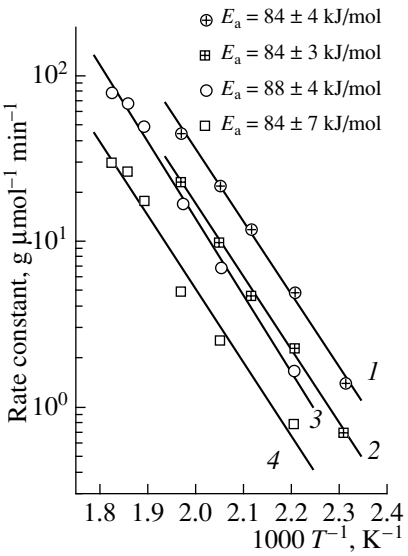

Fig. 11. Arrhenius plots of the H–D exchange rate constant for (*1*, *2*) methane and (*3*, *4*) ethane adsorbed on zeolite ZnHBEA: (*1*, *3*) $k_{(SiOHAl)_1}$ and (*2*, *4*) $k_{(SiOHAl)_2}$.

panied by a weakening of the signals from hydrogen in the two types of Al–OH–Si bridges involved in hydrogen exchange.

By analysis of the temperature dependence of the rate constants of exchange in methane and ethane, it was found that the apparent activation energy of these reactions is 84–88 kJ/mol (Fig. 11). This value is 40–70 kJ/mol lower than the activation energy of H–D exchange on the pure acid forms of zeolites [44–46].

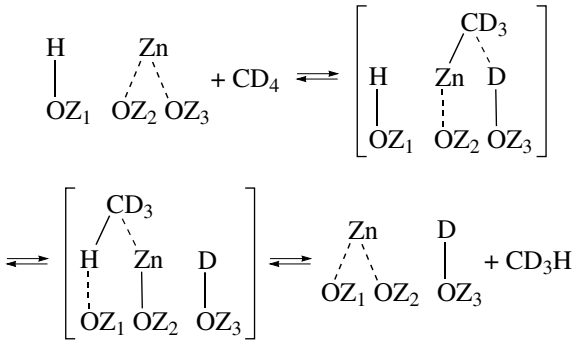

Scheme 7. Possible mechanism of H–D exchange in methane adsorbed on zeolite ZnHBEA.

The lower activation energy and the much lower temperature range of H–D exchange in the case of ZnHBEA suggest that zinc in the zeolite exerts an obvious promoting effect on hydrogen exchange. The mechanism of the reaction on the zinc-containing zeolite must differ significantly from the conventional mechanism of hydrogen exchange on the pure acid forms of zeolites [24, 47–49].

In Scheme 7, we present a possible mechanism of H–D exchange between methane (ethane) and ZnHBEA taking into account the effect of zinc in the zeolite on the reaction kinetics. It is assumed in this mechanism that the alkane undergoes dissociative adsorption on zinc cations located on two adjacent [50] or distant [51] oxygen atoms of the zeolite lattice to yield zinc–alkyl fragments [41–43]. The reversible formation of these garments, which vacates a Brøsted acid

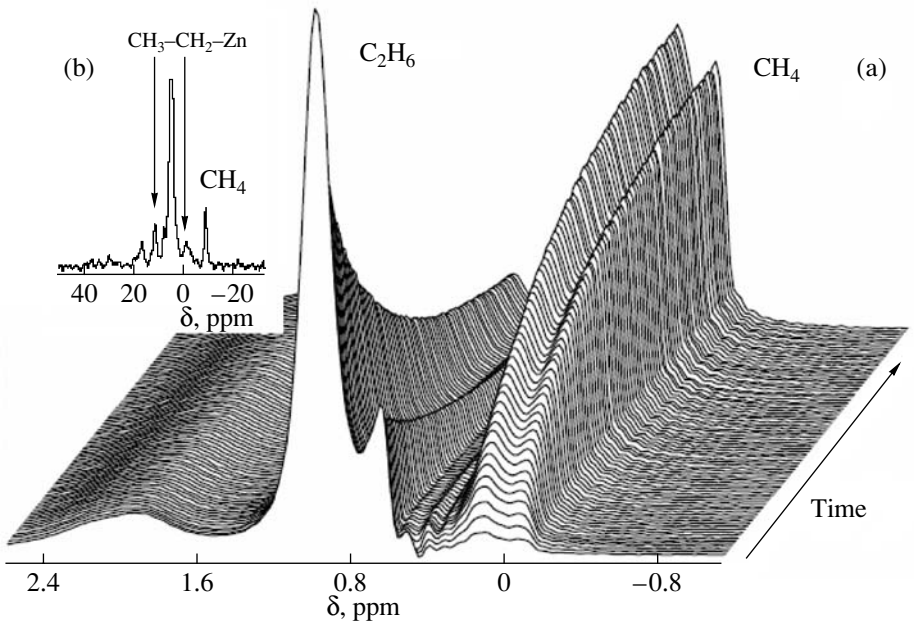

Fig. 12. (a) Time evolution of the ^{1}H MAS NMR spectrum of ethane adsorbed on ZnHBEA. (b) ^{13}C MAS NMR spectrum of ethane ^{13}C-labeled in the 1-position on ZnHBEA 1 h after the beginning of the reaction. The reaction temperature is 573 K.

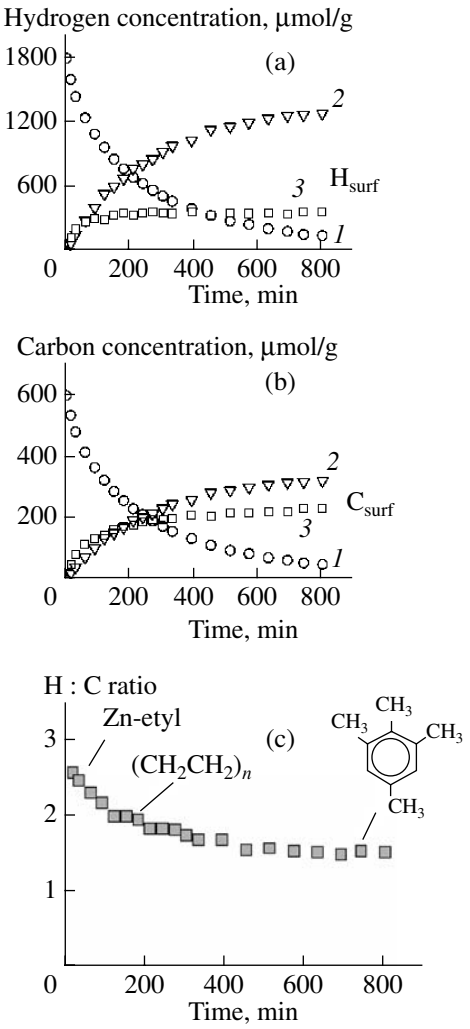

Fig. 13. Variation of the (a) hydrogen and (b) carbon atom concentrations in (*1*) ethane, (*2*) methane, and (*3*) the products undetectable by ^{1}H MAS NMR during ethane conversion on the ZnHBEA surface at 573 K. (c) Variation of the H : C ratio in the undetectable products and possible products corresponding to particular H : C ratios.

site, and the location of the uninvolved Al–OH–Si groups in the immediate vicinity of these fragments are favorable for proton transfer from an Al–OH–Si bridge to a deuterated alkane molecule.

ETHANE AROMATIZATION ON THE ZINC-CONTAINING CATALYST ZnHBEA

Our investigation of high-temperature ethane conversion on zeolite ZnHBEA illustrates the potential of ^{1}H MAS NMR spectroscopy for the in situ identification of reaction products and for revealing mechanistic details of the aromatization of lower alkanes on Zn-containing zeolites.

In situ kinetic monitoring of ethane conversion on ZnHBEA demonstrated that the only product detectable by this method is methane (Fig. 12a). At the same time, an analysis of the variation of the intensity ratio between the ^{1}H NMR signals from initial ethane and resulting methane enabled us to monitor the buildup of carbon and hydrogen atoms in the products that are undetectable by this method and to determine the hydrogen-to-carbon atomic ratio in these undetectable products at all stages of the process (Fig. 13). At the early stages of ethane conversion, the H : C ratio is 2.5, apparently indicating the formation of ethyl fragments on the surface. The subsequent decrease of this ratio to 2.0 can be due to the formation of ethylene or its oligomerization products on the surface. The ultimate H : C ratio is 1.4. This value indicates the formation of aromatic compounds, most likely tetramethylbenzenes.

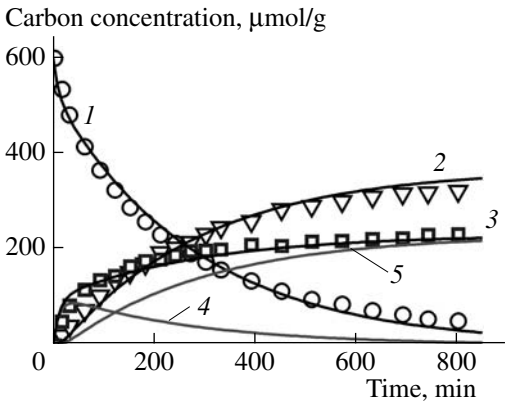

Fig. 14. Experimental (points) and calculated (solid lines) kinetic curves corresponding to the mechanism presented in Scheme 8 for ethane aromatization on zeolite ZnHBEA at 573 K: (*1*) ethane, (*2*) methane, (*3*) surface carbon in the intermediates and products, (*4*) CH_3CH_2–Zn–H, and (*5*) $C_{10}H_{14}$.

POSSIBLE H–D EXCHANGE MECHANISM FOR METHANE ON ZEOLITE ZnHBEA

It was found that only half of the initial ethane is converted into useful aromatic products. The other half is converted into methane. ^{13}C MAS MR spectroscopy confirmed the formation of zinc–ethyl fragments, with characteristic resonances at –0.4 ppm (CH_2) and 12.1 ppm (CH_3), on the catalyst surface at the initial moment of the reaction (Fig. 12b). The release of large amounts of methane can be due to ethane hydrogenolysis proceeding in the same way as propane hydrogenolysis on ZnHZSM-5, the possibility of which was demonstrated earlier [52].

From these data, we derived a kinetic scheme for the initial stage of the aromatization reaction (Scheme 8). This scheme includes the formation of a Zn–ethyl fragment and the subsequent decomposition of this fragment into ethylene and hydrogen. Ethylene is then converted into aromatic products, and the resulting hydrogen can participate in ethane hydrogenolysis.

$C_2H_6 \leftrightarrow [C_2H_5–Zn–H]$ $k_1 = 0.015$ min^{-1}; $k_{-1} = 0.08$ min^{-1}

$[C_2H_5–Zn–H] \rightarrow C_2H_4 + H_2$ $k_2 = 0.008$ min^{-1}

$C_2H_6 + H_2 \rightarrow 2CH_4$ $k_3 = 0.005$ g μmol min^{-1}

$C_2H_4 \rightarrow 1/5C_{10}H_{14} + 3/5H_2$ $k_4 = 0.1$ min^{-1}

The rate constants are calculated for $T = 573$ K. The kinetic scheme calculations were carried out by S.S. Arzumanov.

Scheme 8. Possible mechanism of ethane aromatization on ZnHBEA.

A numerical analysis of this kinetic scheme indicated that the scheme is in good agreement with the experimental data obtained at 573 K (Fig. 14). From the temperature dependences of the rate constants of hypothetical reaction steps, we derived the apparent activation energies of these steps (Fig. 15). The kinetic parameters thus determined for the mechanism presented in Scheme 8 indicate that the rate of the overall reaction is determined by the rate of Zn–ethyl fragment decomposition into ethylene and dihydrogen.

Thus, this in situ NMR study suggested a mechanism for ethane conversion into aromatic products and methane on the Zn-containing zeolite. This mechanism includes the intermediate formation of Zn–ethyl fragments, and this is in agreement with the observed ethane conversion kinetics.

Applying in situ high-resolution solid-state NMR spectroscopy (MAS NMR) to the monitoring hydrocarbon conversion on the surface of heterogeneous catalysts provides valuable information that can help elucidate the hydrocarbon activation and conversion mechanisms. At present, in situ kinetic NMR studies can be performed at rather high temperatures up to 300°C. This circumstance substantially widens the variety of reactions that can be examined. In situ NMR spectroscopy has opened up the unique possibility of studying the conversion kinetics of individual fragments of hydrocarbons. Measuring resonances from different nuclei adds reliability to the deduced reaction mechanisms. The kinetic parameters of elementary reactions determined by this method can provide a basis for theoretically calculating hydrocarbon activation and conversion pathways and for judging the reliability of these calculations.

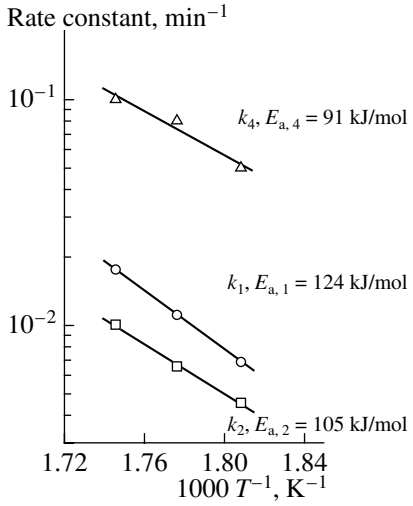

Fig. 15. Arrhenius plots of the rate constants of the reaction steps presented in Scheme 8 for ethane aromatization on zeolite ZnHBEA.

ACKNOWLEDGMENTS

This work was supported by the Russian Foundation for Basic Research (grant no. 04-03-32372), INTAS (grant no. 03-51-5286), and Deutsche Forschungsgemeinschaft (project no. 902/15).

REFERENCES

1. Derouane, E.G., Gilson, J.-P., and Nagy, J.B., *Zeolites*, 1982, vol. 2, no. 1, p. 42.
2. Van den Berg, J.P., Wolthuizen, J.P., Clague, A.D.H., Hays, G.R., Huis, R., and van Hoof, J.H.C., *J. Catal.*, 1983, vol. 80, no. 1, p. 130.
3. Anderson, M.W. and Klinowski, J., *Nature*, 1989, vol. 339, no, 6221, p. 200.
4. Haw, J.F., Richardson, B.R., Oshio, I.S., Lazo, N.D., and Speed, J.A., *J. Am. Chem. Soc.*, 1989, vol. 111, no. 6, p. 2052.
5. Bosacek, V., *J. Phys. Chem.*, 1993, vol. 97, no. 41, p. 10732.
6. Murray, D.K., Chang, J.W., and Haw, J.F., *J. Am. Chem. Soc.*, 1993, vol. 115, no. 11, p. 4732.
7. Wang, W., Jiao, J., Jiang, Y.J., Ray, S.S., and Hunger, M., *ChemPhysChem*, 2005, vol. 6, no. 8, p. 1467.
8. Stepanov, A.G., Romannikov, V.N., and Zamaraev, K.I., *Catal. Lett.*, 1992, vol. 13, no. 4, p. 395.
9. Stepanov, A.G., Zamaraev, K.I., and Thomas, J.M., *Catal. Lett.*, 1992, vol. 13, no. 4, p. 407.
10. Oliver, F.G., Munson, E.J., and Haw, J.F., *J. Phys. Chem.*, 1992, vol. 96, no. 20, p. 8106.
11. Goguen, P.W., Xu, T., Barich, D.H., Skloss, T.W., Song, W., Wang, Z., Nicholas, J.B., and Haw, J.F., *J. Am. Chem. Soc.*, 1998, vol. 120, no. 11, p. 2650.
12. Stepanov, A.G., Sidelnikov, V.N., and Zamaraev, K.I., *Chem. Eur. J.,* 1996, vol. 2, no. 2, p. 157.
13. Luzgin, M.V., Stepanov, A.G., Shmachkova, V.P., and Kotsarenko, N.S., *J. Catal.*, 2001, vol. 203, no. 2, p. 273.

14. Luzgin, M.V., Romannikov, V.N., Stepanov, A.G., and Zamaraev, K.I., *J. Am. Chem. Soc.*, 1996, vol. 118, no. 44, p. 10 890.
15. Luzgin, M.V. and Stepanov, A.G., *Mendeleev Commun.*, 1996, vol. 6, no. 6, p. 238.
16. Stepanov, A.G. and Luzgin, M.V., *Chem. Eur. J.*, 1997, vol. 3, no. 1, p. 47.
17. Derouane, E.G., Hamid, S.B.A., Ivanova, I.I., Blom, N., and Hojlund-Nielsen, P.E., *J. Mol. Catal.*, 1994, vol. 86, nos. 1–3, p. 371.
18. Stepanov, A.G., *Catal. Today*, 1995, vol. 24, no. 3, p. 341.
19. Stepanov, A.G., Luzgin, M.V., Arzumanov, S.S., Ernst, H., and Freude, D., *J. Catal.*, 2002, vol. 211, no. 1, p. 165.
20. Luzgin, M.V., Arzumanov, S.S., Shmachkova, V.P., Kotsarenko, N.S., Rogov, V.A., and Stepanov, A.G., *J. Catal.*, 2003, vol. 220, no. 1, p. 233.
21. Luzgin, M.V., Stepanov, A.G., Arzumanov, S.S., Rogov, V.A., Parmon, V.N., Wang, W., Hunger, M., and Freude, D., *Chem. Eur. J.*, 2006, vol. 12, no. 2, p. 457.
22. Ipatieff, V.N. and Pines, H., *J. Org. Chem.*, 1936, vol. 1, no. 5, p. 464.
23. Stepanov, A.G., Ernst, H., and Freude, D., *Catal. Lett.*, 1998, vol. 54, nos. 1–2, p. 1.
24. Blaszkowski, S.R., Nascimento, M.A.C., and van Santen, R.A., *J. Phys. Chem.*, 1996, vol. 100, no. 9, p. 3463.
25. Haouas, M., Walspurger, S., Taulelle, F., and Sommer, J., *J. Am. Chem. Soc.*, 2004, vol. 126, p. 599.
26. Haouas, M., Walspurger, S., and Sommer, J., *J. Catal.*, 2003, vol. 215, no. 1, p. 122.
27. Stepanov, A.G., Arzumanov, S.S., Ernst, H., and Freude, D., *Chem. Phys. Lett.*, 2006, vol. 420, nos. 4–6, p. 574.
28. Stepanov, A.G., Arzumanov, S.S., Luzgin, M.V., Ernst, H., Freude, D., and Parmon, V.N., *J. Catal.*, 2005, vol. 235, no. 1, p. 221.
29. Arzumanov, S.S., Reshetnikov, S.I., Stepanov, A.G., Parmon, V.N., and Freude, D., *J. Phys. Chem. B*, 2005, vol. 109, no. 42, p. 19 748.
30. Saunders, M., Hewett, A.P., and Kronja, O., *Croat. Chim. Acta*, 1992, vol. 65, no. 3, p. 673.
31. Stepanov, A.G., Arzumanov, S.S., Luzgin, M.V., Ernst, H., and Freude, D., *J. Catal.*, 2005, vol. 229, no. 1, p. 243.
32. Teraishi, K., *J. Mol. Catal. A: Chem.*, 1998, vol. 132, no. 1, p. 73.
33. Boronat, M., Viruela, P.M., and Corma, A., *J. Am. Chem. Soc.*, 2004, vol. 126, no. 10, p. 3300.
34. Saunders, M., Hagen, E.L., and Rosenfeld, J., *J. Am. Chem. Soc.*, 1968, vol. 90, no. 24, p. 6882.
35. Matsuhashi, H., Shibata, H., Nakamura, H., and Arata, K., *Appl. Catal., A*, 1999, vol. 187, no. 1, p. 99.
36. Stepanov, A.G., Luzgin, M.V., Arzumanov, S.S., Wang, W., Hunger, M., and Freude, D., *Catal. Lett.*, 2005, vol. 101, nos. 3–4, p. 181.
37. Ono, Y., *Catal. Rev. Sci. Eng.*, 1992, vol. 34, no. 3, p. 179.
38. Biscardi, J.A., Meitzner, G.D., and Iglesia, E., *J. Catal.*, 1998, vol. 179, no. 1, p. 192.
39. Biscardi, J.A. and Iglesia, E., *J. Catal.*, 1999, vol. 182, no. 1, p. 117.
40. Hagen, A. and Roessner, F., *Catal. Rev. Sci. Eng.*, 2000, vol. 42, no. 4, p. 403.
41. Kazansky, V.B., Serykh, A.I., and Pidko, E.A., *J. Catal.*, 2004, vol. 225.
42. Kazansky, V.B. and Pidko, E.A., *J. Phys. Chem. B*, 2005, vol. 109, no. 6, p. 2103.
43. Kazansky, V.B., Subbotina, I.R., Rane, N., van Santen, R.A., and Hensen, E.J.M., *Phys. Chem. Chem. Phys.*, 2005, vol. 7, no. 16, p. 3088.
44. Larson, J.G. and Hall, W.K., *J. Phys. Chem.*, 1965, vol. 69, no. 9, p. 3080.
45. Lee, B., Kondo, J.N., Wakabayashi, F., and Domen, K., *Catal. Lett.*, 1999, vol. 59, no. 1, p. 51.
46. Schoofs, B., Martens, J.A., and Schoonheydt, R.A., *J. Catal.*, 1999, vol. 183, no. 2, p. 355.
47. Blaszkowski, S.R., Jansen, A.P.J., Nascimento, M.A.C., and van Santen, R.A., *J. Phys. Chem.*, 1994, vol. 98, no. 49, p. 12 938.
48. Zheng, X. and Blowers, P., *J. Mol. Catal. A: Chem.*, 2005, vol. 242, no. 1, p. 18.
49. Zheng, X. and Blowers, P., *J. Mol. Catal. A: Chem.*, 2006, vol. 246, nos. 1-2, p. 1.
50. Frash, M.V. and van Santen, R.A., *Phys. Chem. Chem. Phys.*, 2000, vol. 2, no. 5, p. 1085.
51. Zhidomirov, G.M., Shubin, A.A., Kazansky, V.B., and van Santen, R.A., *Theor. Chem. Acc.*, 2005, vol. 114, nos. 1–3, p. 90.
52. Kolyagin, Y.G., Ordomsky, V.V., Khimyak, Y.Z., Rebrov, A.I., Fajula, F., and Ivanova, I.I., *J. Catal.*, 2006, vol. 238, no. 1, p. 122.